J Appl Electrochem (2011) 41:1201–1213
DOI 10.1007/s10800-011-0313-0

ORIGINAL PAPER

Chemical and mechanical degradation of sulfonated poly(sulfone) membranes in vanadium redox flow batteries

Soowhan Kim · Timothy B. Tighe · Birgit Schwenzer · Jingling Yan · Jianlu Zhang · Jun Liu · Zhenguo Yang · Michael A. Hickner

Received: 20 December 2010 / Accepted: 17 April 2011 / Published online: 3 May 2011

Abstract A sulfonated poly(sulfone) (S-Radel®) membrane with high proton conductivity and low vanadium ion permeability showed high initial performance in a vanadium redox flow battery (VRFB) but suffered mechanical and chemical degradation during charge/discharge cycling. The S-Radel membrane showed different degradation behavior in flow cell cycling and ex-situ vanadium ion immersion tests. When the membrane was immersed in aqueous V^{5+} solution, the sample cracked into small pieces, but did not degrade to any measurable extent in V^{4+} solution. During charge/discharge cycling in the VRFB cell, the membrane underwent internal delamination, preferentially on the side of the membrane that faced the positive electrode. A vanadium-rich region was observed near the membrane surface that experienced delamination and Raman spectroscopic analysis of the degraded surface indicated a slightly depressed 1026 cm^{-1} band corresponding to a loss in the sulfonate SO_2 stretch intensity. Even though the S-Radel membrane underwent severe mechanical damage during the flow cell cycling, significant chemical degradation was not obvious from the spectroscopic analyses. For the VRFB containing an S-Radel membrane, an increase in membrane resistance caused an abnormal voltage depression during the discharge cycle. The reversible increase in membrane resistance and severe mechanical degradation of the membrane during cycling may be attributed to repeated formation and dissolution of particles inside the membrane. The mechanical stresses imposed by the particles coupled with a small amount of chemical degradation of the polymer by V^{5+} ions, are likely degradation mechanisms of the S-Radel membrane in VRFBs under high state-of-charge conditions.

Keywords Degradation · Poly(sulfone) membrane · Vanadium · Membrane · Redox flow battery

1 Introduction

Electricity generation from renewable sources, for example sun and wind, has been increasing because of growing environmental concerns about fossil fuels and limited hydrocarbon reserves. The intermittent nature of renewable energy requires large-scale electrical energy storage devices to provide stable and reliable electricity in concert with existing power grids. Among the promising technologies for grid-scale energy storage are redox flow batteries [1]. Flow batteries store energy in liquid electrolytes that contain reversible redox couples and have desirable attributes of long life, active thermal management, and independent energy and power ratings depending on their configuration [2]. Particularly the all-vanadium redox flow battery (VRFB) has received much attention because of its good electrochemical reversibility, high efficiency, and absence of cross-contamination between the anolyte and catholyte [3, 4]. Multi-MWh VRFB systems have been demonstrated for grid and renewable applications and have shown great potential to improve the reliability and efficiency of utility transmission and distribution networks

Pacific Northwest National Laboratory (PNNL) is a multiprogram laboratory operated by Battelle Memorial Institute for the Department of Energy under Contract DE-AC05-76RL01830.

S. Kim (✉) · B. Schwenzer · J. Zhang · J. Liu · Z. Yang
Pacific Northwest National Laboratory, Richland, WA 99352, USA
e-mail: soowhan.kim@pnl.gov

T. B. Tighe · J. Yan · M. A. Hickner (✉)
Department of Materials Science and Engineering, The Pennsylvania State University, University Park, PA 16802, USA
e-mail: hickner@matse.psu.edu

[2]. The VRFB technology is still expensive and has drawbacks including relatively low energy density resulting from limited solubility of the vanadium compounds in aqueous solutions and limited thermal stability of the electrolyte. Therefore, continued efforts to reduce the cost and improve the energy density are required to realize wide-spread deployment of this technology.

The VRFB employs the redox couples, VO^{2+}/VO_2^+ and V^{2+}/V^{3+} in aqueous sulfuric acid solution as positive and negative half-cells, respectively. The two half-cells, with the reactions occurring on carbon cloth or carbon felt electrodes, are separated by a proton exchange membrane, which physically separates the positive solution (anolyte) and the negative solution (catholyte), preventing self-discharge while allowing proton transfer to complete the circuit. The demands for the membrane are stringent: low transport of vanadium ions, low ionic resistance, low cost, and good longevity in the presence of the electrolyte solutions. A high proton conductivity and low vanadium ion crossover, e.g. high electrochemical selectivity [5], increases the device's coulombic efficiency, leading to high overall efficiency. In this type of cell, the ohmic loss due to the membrane dominates the cell voltage (ohmic losses account for 50–60% of total voltage loss) [6], thus a low ionic membrane resistance would enable high current operation of the device, which can reduce the system's overall cost by reducing the device size. The carbon electrodes show no or very little corrosion during cycling, and the anolyte and catholyte solutions do not degrade during the lifetime of the VRFB if they are kept oxygen free. Thus, the life of the VRFB is determined by longevity of the membrane, which must sustain its performance for 10 years or longer [2].

Nafion is widely employed as a membrane in VRFBs because of its good chemical stability, high proton conductivity, and commercial availability. However, Nafion is expensive (membranes make up 41% of flow cell stack cost [2]) and has high vanadium ion transport. VRFBs with Nafion membranes have suffered from low coulombic efficiency and capacity fade during repeated cycling [7, 8]. Periodic rebalancing of the electrolyte solutions is required by mixing of the anolyte and catholyte solutions to recover the capacity, which increases the operational cost of the device. To improve the selectivity of vanadium ions, modification of Nafion membranes, for example by inorganic doping and surface coating, has been attempted [9–12], but Nafion membrane modifications do not mitigate the cost concerns.

Among alternative proton exchange membranes to Nafion, sulfonated aromatic polymer membranes show sufficient ion conductivity at high hydration, low molecular and ion permeability, and reasonable mechanical and chemical stability in polymer electrolyte fuel cells [13]. Sulfonated aromatic polymer membranes may improve the VRFB's performance by virtue of their low crossover of vanadium ions and they may improve the economics of flow batteries by decreasing the membrane cost compared to Nafion. Recently, researchers have directed much attention towards these alternative membranes for use in a VRFB [7, 14–18], and many candidates have shown promising performance, but their durability has not yet been validated. Most investigations do not report cell performance beyond 80 cycles, which is not sufficient to prove the long-term durability of these materials. Recent results and test conditions are summarized in Table 1.

Mohammadi and Skyllas-Kazacos [20] investigated the long-term chemical stability of Daramic®, divinylbenzene (DVB) cross-linked Daramic, Selemion® CMV (Asahi Glass Co., Japan, cation exchange membrane), Selemion® AMV (Ashai Glass Co., Japan, anion exchange membrane), sulfonated AMV, and Nafion 112 membranes at ambient temperature by immersing the samples in 0.1 and 2.0 M V^{5+} sulfuric acid solutions, a highly oxidative condition that mimics operation in a VRFB. The 2.0 M V^{5+} solution was prepared by electrochemically oxidizing 2.0 M $VOSO_4$ in 3.0 M H_2SO_4 solution, and the 0.1 M V^{5+} solution was prepared by dilution of the 2.0 M V^{5+} solution. They quantified the oxidation of the membrane by measuring the concentration of V^{4+}, resulting from a reduction reaction of V^{5+} to V^{4+}, of the solutions containing the membrane samples with time by UV/Vis spectroscopy. Test results are summarized in Table 1. Except for the perfluorinated membranes (e.g. Nafion® and Gore-Select®), the tested membranes suffered from severe oxidation (>23% reduction of V^{5+} to V^{4+}) with accompanying weight loss: CMV was the worst performer (66% reduction of V^{5+} to V^{4+} and 54% weight loss) followed by the Daramic micro-porous separator (33% reduction of V^{5+} to V^{4+}). For Selemion membranes, the CMV membrane was much more oxidized than the AMV membrane, and cross-linking with the addition of DVB in the composite Daramic membrane enhanced its chemical stability. In all tested samples, the membrane resistance decreased and the ion exchange capacity (IEC) and the vanadium ion diffusivity increased. The changes in the membrane properties could be attributed to increased membrane swelling as a result of polymer dissolution resulting from the oxidation of the polymer by V^{5+} in solution. In long-term charge/discharge cycling tests, the Nafion 112 was susceptible to fouling by ion exchange with vanadium species, which caused a significant increase in the membrane resistance. However, this fouling was recovered by immersion in sulfuric acid solution to reprotonate the sample.

Sukkar and Skyllas-Kazacos [8] conducted long-term (60 and 120 days) chemical stability tests of Gore-Select membranes (cation exchange membrane), Selemion® Type 3H (anion exchange membrane), and Nafion 112 membranes, as summarized in Table 1. The Nafion membrane underwent the most oxidation in the 0.1 M V^{5+} solution as evidenced by the highest V^{4+} concentration resulting from the membrane oxidation, but showed good stability in the 1.0 M V^{5+} solution. In addition, the ionic resistance decreased and

Table 1 Summary of durability tests of membranes for VRFBs

Membranes	Test conditions	Results
SPEEK [15]	Cycling (1.65/0.8 V, 50 mA cm^{-2}), 1.5 M V ion, 80 cycles	Slight efficiency loss, no holes but small dents on membrane surface
Nafion/SPEEK [9]	Cycling (1.75/0.8 V) 1.5 M V ion, 30 cycles	Stable efficiencies
SPES [16]	Fenton solution (3 wt% H_2O_2 + 2 ppm $FeSO_2$), 80 °C	Breakage start after 220 h, membrane disappear after 260 h
S-Radel [7, 19]	Cycling (1.7/0.8 V, 50 mA cm^{-2}), 2.0 M V, 45 cycles	Abrupt efficiency loss after 41 cycle Mechanical delamination
Selemion® CMV [20]	Soaking (0.1 M V^{5+}), 60 days	Weight loss (54%), $V^{5+} \rightarrow V^{4+}$ (66%)
Selemion® AMV [20]	Soaking (0.1 M V^{5+}), 60 days	Weight loss (6%), $V^{5+} \rightarrow V^{4+}$ (23%)
S-AMV [20]	Soaking (0.1 M V^{5+}), 60 days	Weight loss (15%), $V^{5+} \rightarrow V^{4+}$ (30%)
	Soaking (2 M V^{5+}), 180 days	R (Ω cm^2) decrease (2.54 → 1.79)
Daramic® [20]	Soaking (0.1 M V^{5+}), 60 days	Weight loss (23%), $V^{5+} \rightarrow V^{4+}$ (33%)
S-Daramic/DVB [20]	Soaking (0.1 M V^{5+}), 60 days	Weight loss (18%), $V^{5+} \rightarrow V^{4+}$ (32%)
	Cycling (30 mA cm^{-2}), 2 M V ion, 1950 cycles (180 days)	R (Ω cm^2) decrease (2.52 → 2.21), diffusivity increase (53%)
Nafion 112 [8, 20]	Soaking (0.1 M V^{5+}), 120 days	$V^{5+} \rightarrow V^{4+}$ (8%), R (Ω cm^2) decrease (57%), IEC (mmol g^{-1}) increase (1.5 → 3.6), diffusivity increase (237%)
	Soaking (2 M V^{5+}), 180 days	R (Ω cm^2) decrease (0.89 → 0.68)
	Cycling (30 mA/cm^2), 2 M V ion, 1950 cycles (180 days)	R (Ω cm^2) increase (0.89 → 1.88), diffusivity up (17%), recoverable fouling
Gore-Select L-570 [8]	Soaking (0.1 M V^{5+}), 120 days	$V^{5+} \rightarrow V^{4+}$ (2%), R (Ω cm^2) decrease (39%), IEC (mmol g^{-1}) increase (2.0 → 5.2), diffusivity up (76%)
Gore-Select L-01009 [8]	Soaking (0.1 M V^{5+}), 120 days	$V^{5+} \rightarrow V^{4+}$ (2%), R (Ω cm^2) decrease (30%), IEC (mmol g^{-1}) increase (1.1 → 2.5), diffusivity increase (7%)
Selemion® Type 3H [8]	Soaking (0.1 M V^{5+}), 60 days	$V^{5+} \rightarrow V^{4+}$ (8%), Negligible R change, IEC (mmol g^{-1}) increase (2.0 → 3.0), negligible diffusivity change
PPR or PANI coated Nafion [12]	Soaking (0.1 M V^{5+}), <7 days	Coating layers dissolved

S-AMV sulfonated Selemion AMV, anion type; *CMV* cation type; *S-Daramic/DVB* sulfonated divynylbenzene-crosslinked Daramic composite; *SPEEK* sulfonated poly(tetramethydiphenyl ether ether ketone), *Nafion/SPEEK* Nafion-coated sulfonated poly(ether ether ketone), *SPES* sulfonated poly(arylene ether sulfone), *PPR* polypyrrole, *PANI* polyaniline, *S-Radel* sulfonated Radel

the IEC and vanadium ion diffusivity increased to different extents for the membranes during the vanadium ion solution immersion tests, but no physical damage was detected by observations with field emission scanning electron microscopy. Selemion Type 3H membranes showed poorer stability in the 1 M V^{5+} solution and Gore-Select membranes showed little oxidation in both solutions. The authors proposed that increased degradation of the membranes correlated with high water swelling and therefore high vanadium ion uptake, which significantly increased the contact between V^{5+} and the polymer. The V^{5+} can easily penetrate into the membrane due to Nafion's high swelling in the dilute V^{5+}/H_2SO_4 solution. This result may indicate that the chemical oxidation of the membrane by V^{5+} may be mitigated by decreasing the water uptake of the membrane for VRFB applications. These authors proposed that the vanadium ion immersion test is suitable for screening materials, but the degradation testing must be conducted in a flow cell under cycling conditions.

Given the initial work, the details of the degradation mechanisms of the polymer during vanadium ion immersion tests as well as during flow cell cycling experiments have not been fully explored. In our previous studies [7, 19], sulfonated poly(sulfone) membranes have shown promising VRFB performance, but degradation of the membrane was observed during charge/discharge cycling experiments. Expanding on the performance studies, we report detailed analysis of the degradation processes for sulfonated poly(sulfone) membranes during flow cell cycling and ex-situ immersion tests.

2 Experimental

2.1 Polymer synthesis and membrane fabrication

Sulfonated Radel (poly(phenylsulfone) Radel® R-5500, MW 63 kg mol^{-1}, donated by Solvay Advanced Polymers, LLC) was prepared by post-sulfonation with trimethylsilyl

chlorosulfonate (Aldrich, 99%) in tetrachloroethane (Aldrich, >98%) [21]. The ion exchange capacity of the resulting sulfonated polymer was determined to be 1.95 meq g^{-1} using ^1H NMR in DMSO-d6. Membranes were fabricated by casting S-Radel/dimethylformamide (DMF, Mallinckrodt Analytical) solutions onto glass plates and drying at 60 °C for 2 h, then 80 °C for 2 h in an atmospheric environment, followed by drying in a vacuum oven at 80 °C for 5 h. The membrane thickness was approximately 0.115 mm. The conductivity of the S-Radel immersed in water at 30 °C was 100 mS cm^{-1}, and the water uptake under the same conditions was 37 wt% [22].

2.2 VRFB cell testing

Discharge rate and charge/discharge cyclic performance of S-Radel membranes were evaluated using an in-house designed flow cell system. The system included a single cell, two peristaltic pumps, two electrolyte reservoirs, and Viton® tubing. The anolyte and catholyte flow rates were 20 mL min^{-1} and the two electrolyte reservoirs were sealed to minimize oxidation of the vanadium species. Pieces of graphite felt, GFD5 (SGL Carbon Group, Germany), with projected areas of 10 cm^2 were used as the porous electrodes. The felt was thermally oxidized for 6 h at 400 °C in air to enhance its electrochemical activity and hydrophilicity. The details of the single cell are described in Ref. [7].

The starting electrolyte was prepared by dissolving $VOSO_4 \cdot 3.8H_2O$ (Sigma-Aldrich, 97%) in sulfuric acid. 1.7 M VO_2^+ and 1.7 M V^{2+} in 5.0 M total sulfate were prepared by electrochemical oxidation of 1.7 M $VOSO_4$ in 5.0 M total sulfate. Each electrolyte solution volume was 50 mL during flow cell testing.

Multiple flow cells were assembled using S-Radel membranes, and cycling tests were carried out using a multichannel potentiostat (BT2000, Arbin Instruments, TX, USA). The flow cell was cycled between 0.8 and 1.7 V, equivalent to a state of charge (SOC) of 0 and ~100%, respectively, at a current density of 75 mA cm^{-2}. During the cycling, coulomb, energy and voltage efficiencies of the flow cell were monitored and calculated by:

$$\text{Coulombic efficienecy (CE)} = \frac{\int I_d dt}{\int I_c dt} \quad (1)$$

$$\text{Energy efficienecy (EE)} = \frac{\int V_d I_d dt}{\int V_c I_c dt} = \frac{V_{d,avg} \int I_d dt}{V_{c,avg} \int I_c dt} = \frac{V_{d,avg}}{V_{c,avg}} \times \text{CE} \quad (2)$$

$$\text{Voltage efficienecy (VE)} = \frac{V_{d,avg}}{V_{c,avg}} = \frac{\text{EE}}{\text{CE}} \quad (3)$$

where c denotes charging and d indicates discharging. $V_{d,avg}$ and $V_{c,avg}$ represent average discharge voltage and charge voltage, while I_d and I_c are the discharge and charging current. Cells were examined after different numbers of cycles and with cycling to different SOCs as described in Sect. 3.

To investigate the abnormal voltage depression, which the flow cell with S-Radel membrane suffered from during the discharge, the discharge rate capability tests with the S-Radel and Nafion 117 (N117) membranes were conducted and compared. The flow cell was charged to 1.7 V with a current density of 50 mA cm^{-2}, and was discharged to 0.8 V at 25, 50, 75, and 100 mA cm^{-2}. AC impedance, 100 kHz to 1 Hz with an amplitude of 10 mV at open circuit, was carried out on the flow cell at various SOC using a ModuLab® electrochemical system (Model 2100A, Solartron Analytical, UK) to determine the high frequency resistance (HFR) of the cell, which occurred at 5–6 kHz (minimum in imaginary impedance). The HFR of the flow cell was measured at SOC 100% and 90% during cycling at 2 kHz using the multichannel potentiostat (BT2000, Arbin instruments, TX, USA), which gave an HFR 20–30% higher than the true high frequency resistance determined by the ModuLab.

2.3 Ex-situ chemical stability testing

The chemical stability of the membranes was evaluated by immersion in V^{5+} solution similar to the previously reported method [8]. Membrane samples of size 25 mm × 25 mm and electrolyte solutions (29 mL) were placed in sealed poly(tetrafluoroethylene) bottles (30 mL) and held without agitation in a 40 °C water bath or at ambient temperature (~22 °C). The electrolyte solutions were (1) dilute solution with 0.1 M V^{5+} in 5.0 M total sulfate, and (2) concentrated 1.7 M V^{5+} in 5.0 M total sulfate, which is the typical concentration for VRFB application. The 1.7 M V^{5+} solution was prepared by the flow cell operation, and the 0.1 M V^{5+}/5.0 M SO_4^{2-} solution was prepared by diluting the 1.7 M V^{5+}/5.0 M SO_4^{2-} solution with sulfuric acid (95.8%). During the immersion tests, after 5, 10, 24, 50, 82, and 170 h, 2 mL aliquots from the test bottles were removed, and the concentration of V^{4+} (VO^{2+}) was measured by UV/Vis spectroscopy (Shimadzu UV 3600 UV–Vis–NIR Spectrometer; with PMMA cuvettes; the as-prepared 0.1 M V^{5+} in 5.0 M total sulfate solution was used as the blank reference for the measurements) [8]. To investigate the effect of vanadium ion valance on chemical stability, immersion tests (40 °C) in solutions of V^{2+}, V^{3+}, and V^{4+} with 1.7 M vanadium ions in 5.0 M total sulfate were also conducted for the S-Radel membrane. The V^{2+} solution was prepared at the negative pole by charging the flow cell to 1.7 V at 50 mA cm^{-2}, where the anolyte and catholyte were 1.7 M $VOSO_4$ in 3.3 M H_2SO_4 and the anolyte volume was double the catholyte volume to balance the electrical charge. The V^{3+} solution was prepared by mixing equal volumes of the 1.7 M V^{4+} and 1.7 M V^{2+} solutions.

2.4 Membrane analysis

Raman analysis was performed using a confocal Raman microscope (Renishaw inVia, UK) with a 50×/0.75 NA objective, 1200 or 2400 lines mm^{-1} diffraction gratings, 785 nm diode laser, and Peltier-cooled charge-coupled device (CCD). The diode laser (~30 mW at 100% power) was operated at 10% power with a laser defocus of 50% to avoid signal saturation and sample damage. Co-additions of five scans (200–2000 cm^{-1}) and 10 scans (965–1095 cm^{-1}), with an exposure time of 10 s, were used to increase the signal to noise ratios of the spectra. Scanning electron microscope (SEM) images were collected using a FEI Quanta 200 ESEM with an acceleration voltage of 20 kV. Energy dispersive X-ray spectroscopy (EDS) analysis was performed to determine elements of the flow cell cycled and immersion-test membranes using a JEOL JSM-5900 microscope. For EDS analysis across the cross-section of the cycled membrane, the sample was mounted in epoxy and then polished using diamond slurries of different particles sizes, down to 1 μm. Samples were sputter-coated with carbon before analysis.

3 Results and discussion

3.1 Flow cell performance and post-test analyses of cycled membranes

Figure 1a shows that the VRFB with the S-Radel membrane employing 2.0 M V in 5.0 M total sulfate electrolyte had good initial performance, but experienced an abrupt loss in coulombic and energy efficiency after the 41st cycle (460 h total run time) [7]. There was a slight voltage efficiency loss with cycling, but a dramatic decrease in voltage efficiency was not observed even after the 41st cycle when there was a drastic decrease in coulombic and energy efficiencies. The relatively robust voltage efficiency represents little change of average charge and discharge

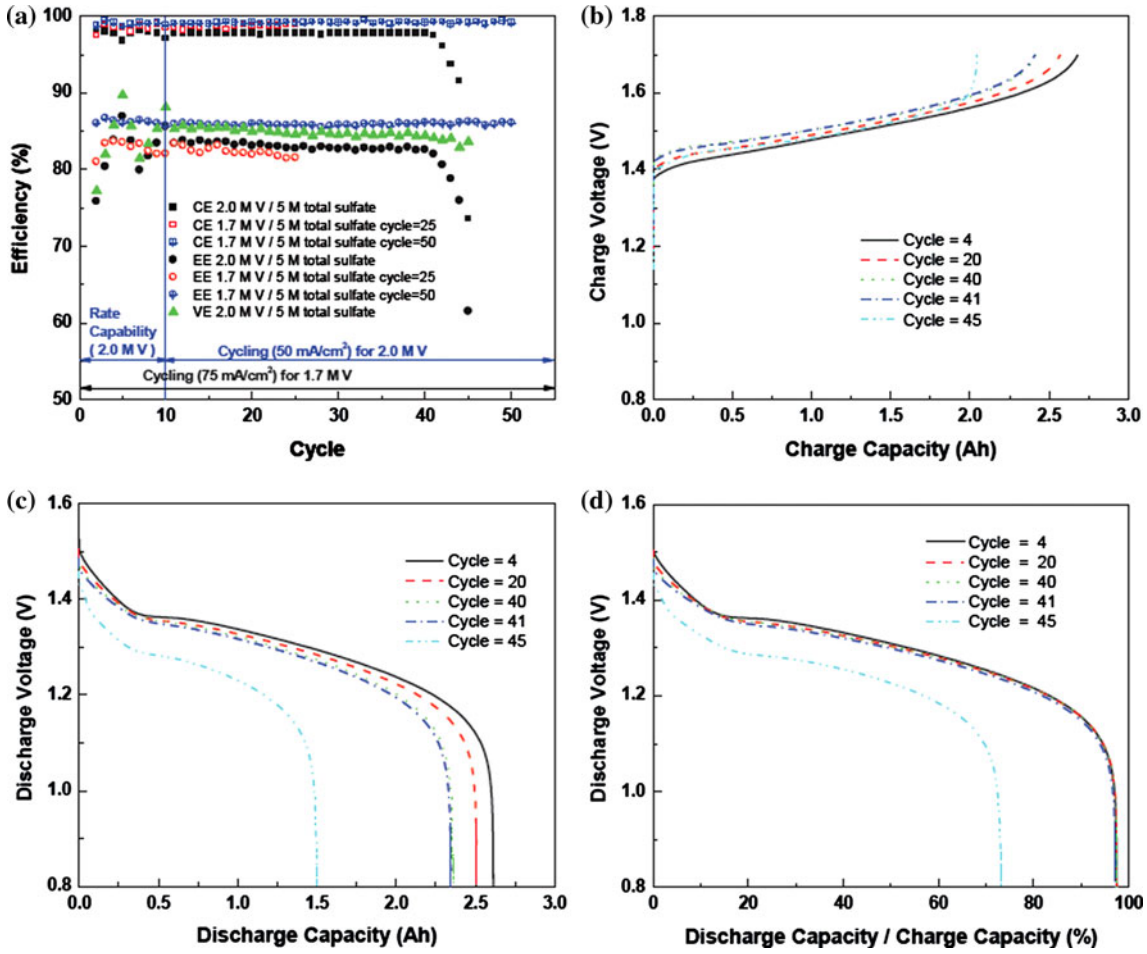

Fig. 1 Cyclic performance of S-Radel membranes with different V concentration (2.0 vs. 1.7 M) in 5.0 M total sulfate solution and current densities (50 mA cm^{-2} for 2.0 M V ion and 75 mA cm^{-2} for 1.7 M V): **a** Coulombic efficiency (CE), voltage efficiency (VE) and energy efficiency (EE) of S-Radel membranes and **b–d** charging and discharging curves with different cycles (i.e. 4, 20, 40, 41, and 45 cycle)

voltage (see Eq. 3) and little change of the cell resistance. The charge and discharge voltage curves (see Fig. 1b–d) with different cycles (i.e. 4, 20, 40, 41 and 45) clearly show that the charge capacity and discharge capacity significantly decreased after the 41st cycle. For the 41st cycle, discharge capacity was 2.35 Ah, 98% of the charge capacity (2.41 Ah), while for the 45th cycle the discharge capacity was 1.51 Ah, 74% of the charge capacity (2.05 Ah). Dramatic coulombic efficiency and capacity loss resulted from drastically increased vanadium ion crossover through the S-Radel membrane. The post-test analysis of the membrane showed that the large decrease in cell performance and increase in vanadium ion crossover was a consequence of macroscopic delamination of the membrane in the active cell area [19].

To understand how the membrane degraded with cycling in the device, additional cycling tests were conducted and post-test analyses were carried out after 25 (125 h run time) and 50 (254 h run time) cycles, where the vanadium concentration was 1.7 M in 5.0 M total sulfate and the charge/discharge current density was 75 mA cm^{-2}. Contrary to the cycling test with 2.0 M V in 5.0 M total sulfate, the flow cell did not show any performance loss for the 25 and 50 cycle tests, indicating that the membrane remained intact.

Figure 2a and b exhibits optical micrographs of the S-Radel membranes immersed in deionized water after disassembly of the flow cells that underwent 25 and 50 charge/discharge cycles. Even though there was no degradation in cell performance, the S-Radel membranes showed significant physical degradation. The S-Radel membrane from the 25 cycle test displayed a relatively smooth surface and no cracks immediately after cell disassembly, but the surface in contact with the positive electrode became rough after immersion in deionized water. The additional swelling of the membrane in deionized water relative to its swelling in electrolyte solution likely promoted small cracks that formed during the

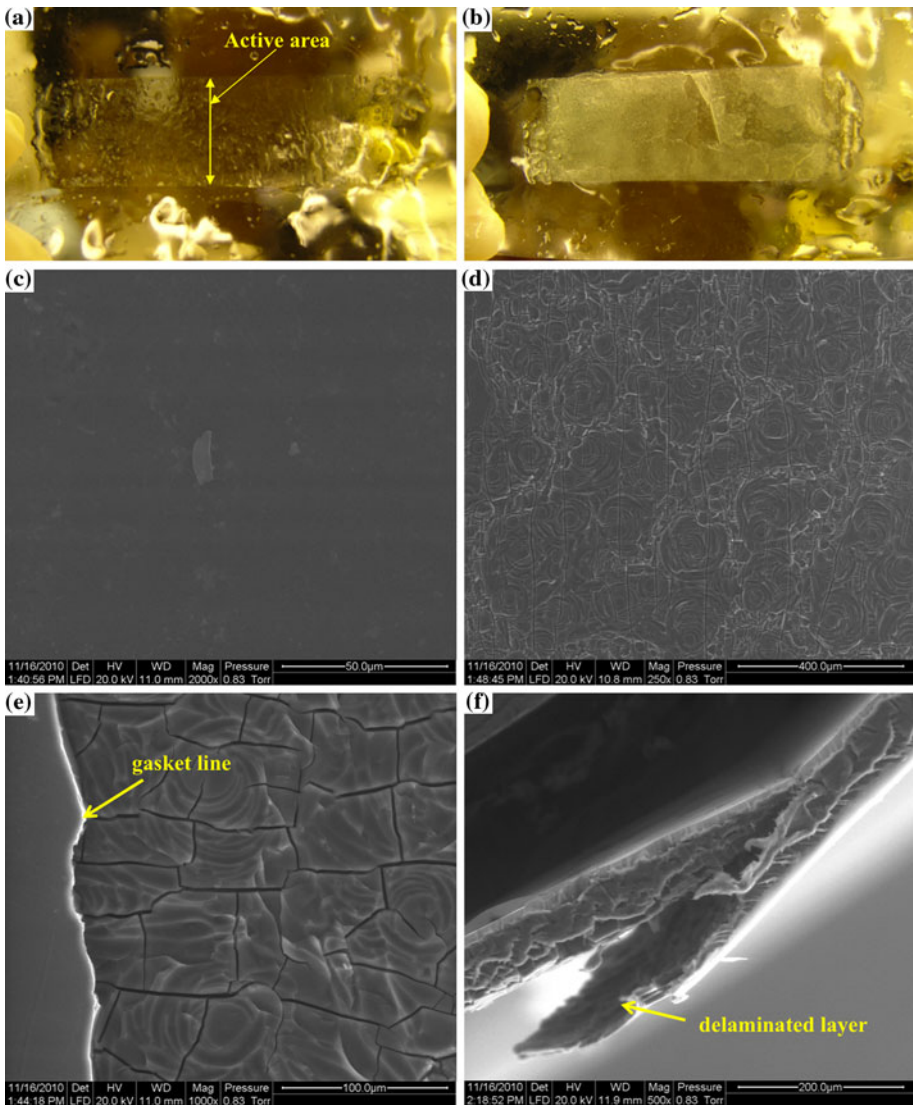

Fig. 2 Optical micrographs of S-Radel membranes cycled in flow cells: **a** 25 cycles; **b** 50 cycles, and scanning electron micrographs of S-Radel after 50 charge/discharge cycles; **c** surface of the membrane facing negative electrode; **d** surface of the membrane facing positive electrode; **e** interface of the gasketed area and active area for positive-facing surface; and **f** delaminated layer on the surface facing the positive electrode

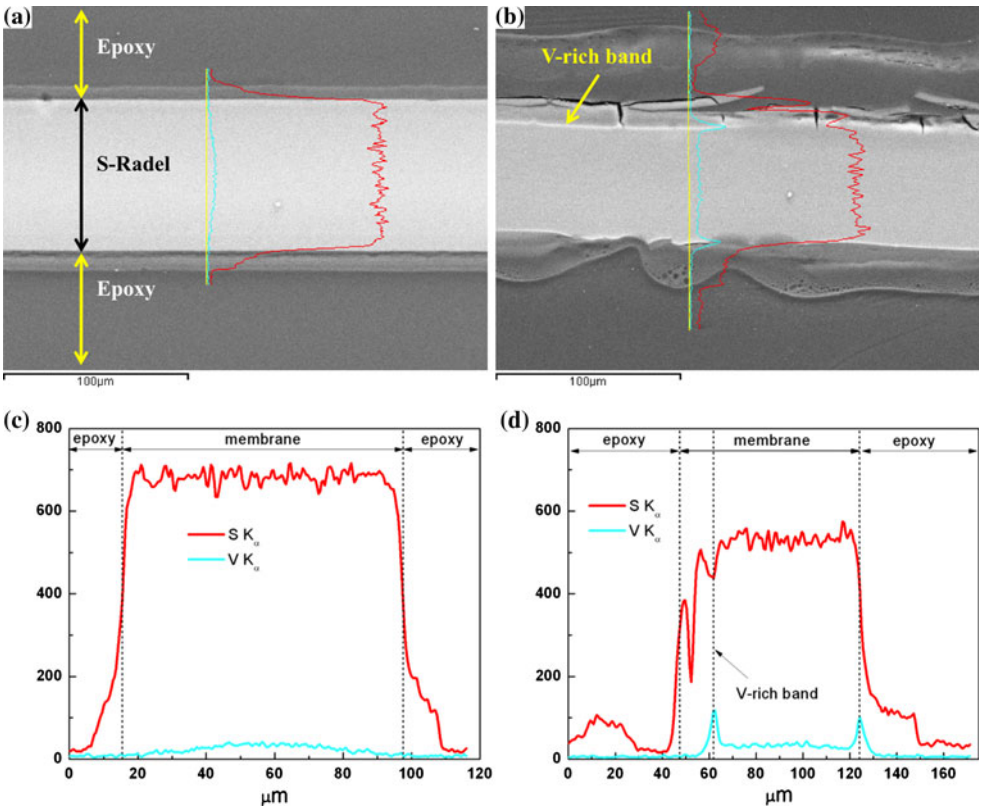

Fig. 3 Cross-sectional scanning electron micrographs with EDS line scans of the S-Radel membrane cycled 50 times, where *V* and *S* intensities are denoted in *cyan* and *red*, respectively: **a** gasketed area; **b** active area; and **c** and **d** are EDS line scans of (**a**) and (**b**), respectively. The membrane surface that faced the positive electrode is facing up in the micrographs. (Color figure online)

cycling test to expand and become visible in the post-test analysis. In comparison, the S-Radel membrane that underwent 50 cycles suffered from severe delamination and surface cracking. On the side of the membrane that was exposed to the positive electrolyte solution, a ~15 μm thick layer was detached across the entire active area.

Compared to the condition of the membrane surface facing the negative electrode (Fig. 2c), surface cracks and delamination are clearly visible on the membrane surface facing the positive electrode (Fig. 2d–f). The gasketed area unexposed to electrolyte solution did not suffer from any observable mechanical damage or chemical degradation (Fig. 2e). Interestingly, the mechanical degradation of the membrane appeared to proceed by a delamination process where "flakes" of the membrane became detached from the sample (Fig. 2f). We have not observed this type of degradation for poly(aromatic) membranes, like S-Radel, in other electrochemical cells, including fuel cells and electrolyzers, previously.

Energy dispersive X-ray spectroscopy line scans of the cross section of the S-Radel membrane that underwent 50 cycles are shown in Fig. 3. The gasketed area showed uniform structure and composition, while the active area revealed a band of high vanadium and low sulfur content, typically ~15 μm beneath the membrane surface on the positive electrode side. It was observed in many cross-sectional SEM micrographs (not shown here) that lateral delamination occurred at or near the vanadium-rich band.

3.2 Ex-situ chemical stability test

Figure 4 shows the color change of 0.1 M V^{5+} solutions containing N117 (40 °C) and S-Radel (40 and ~22 °C) samples as well as blank solution (0.1 M V^{5+} solution without membrane) after 170 h. The color of pure V^{5+} and pure V^{4+} electrolyte is yellow and blue, respectively. The color of the V^{5+} solution containing N117 did not change with time as was observed for the blank solution. V^{4+} ions in the solution containing N117 were not detectable by UV/Vis spectroscopy. In comparison, the solution containing the S-Radel membrane became more green-colored (mixture of yellow and blue) and the amount of V^{4+} ions increased with time as a result of reduction of V^{5+} to V^{4+} (Fig. 4e). The V^{4+} ion concentration in solutions of S-Radel membranes stored at 40 °C was two times greater than that at ambient temperature, indicating that the higher temperature accelerated degradation of the membrane. The change in vanadium ion valence indicated that the membranes were likely oxidized with time as the vanadium species were reduced.

Besides the color change, the S-Radel membrane in the V^{5+} solution broke into small pieces during immersion and the extent of breakage in a 1.7 M V^{5+} solution (control experiment, data not shown here) was higher than that in the 0.1 M V^{5+} solution. The physical breakage of the S-Radel membrane was likely a result of the degradation

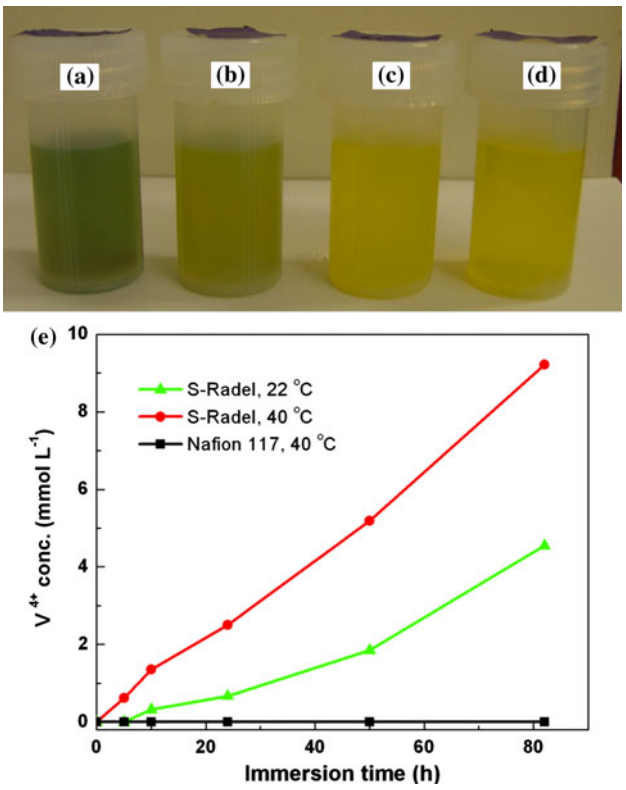

Fig. 4 Electrolyte (0.1 M V^{5+} in 5.0 M total sulfate) solutions and membrane samples after immersion for 170 h: **a** S-Radel at 40 °C; **b** S-Radel, at ambient temperature (~22 °C); **c** Nafion 117, at 40 °C; **d** blank solution; and **e** concentration change of V^{4+} ions with time of solutions containing S-Radel membranes at ambient and 40 °C, respectively; concentration of V^{4+} ions in solution at 40 °C containing Nafion 117 is plotted as a reference

processes in solution causing a decrease in the polymer molecular weight, similar to what is observed for sulfonated poly(aromatic) membranes degraded under oxidative conditions by peroxide or hydroperoxide radicals [23].

Oxidation of the S-Radel membrane was exacerbated with high V^{5+} concentration. For a membrane with high swelling in solution, the membrane oxidation is expected to increase with concentration as a result of more contact between the polymer chains and V^{5+}. The oxidation power of the vanadium ion solution can be estimated by the solution potential, or in this case, the equilibrium potential of V^{4+}/V^{5+} redox couple as expressed by Eq. 4:

$$E^{eq} = E^{\circ} - \frac{RT}{F}\ln\frac{(a_{VO^{2+}}\, a_{H_2O})}{a_{VO_2^+}\, a_{H^+}^2} \approx E^{\circ} - \frac{RT}{F}\ln\frac{(c_{VO^{2+}})}{c_{VO_2^+}\, c_{H^+}^2}$$
$$= E^{\circ} - \frac{RT}{F}\ln\left(\left(\frac{c_{VO_2^+,\,t=0}}{c_{VO_2^+}} - 1\right)\frac{1}{c_{H^+}^2}\right) \quad (4)$$

where E^{eq} is the equilibrium potential, E° is the standard potential (1.0 V), R denotes the ideal gas constant (8.314 J mol^{-1} K^{-1}), F is Faraday's constant (96,485 C mol^{-1}), a_i stands for the activity of species i, c_i is the concentration of species i, and $c_{i,t=0}$ denotes the initial concentration of species i. A higher equilibrium potential describes a more oxidizing solution, which is caused by a high concentration of V^{5+} ions as described by Eq. 4. For a fixed volume of electrolyte and a fixed size of membrane, the V^{5+} ion concentration decreases with time as a result of polymer oxidation, and the V^{4+} ion concentration increases. The solution potential for 1.7 M V^{5+} solution containing the S-Radel membrane for 154 h at 40 °C was 1.210 V (~97% SOC) whereas the 0.1 M V^{5+} solution had a solution potential of 1.177 V (~87% SOC) vs. NHE (after 154 h immersion at 40 °C). While the solution potentials do not vary greatly with the V^{5+} concentration, the higher species concentration in the 1.7 M V^{5+} solution results in much more membrane degradation in the immersion tests.

Unlike the V^{5+} solution test, S-Radel membranes immersed in V^{2+}, V^{3+}, and V^{4+} with 1.7 M V in 5.0 M total sulfate remained flexible and did not undergo breakage during prolonged exposure to vanadium ions. Figure 5 shows scanning electron micrographs of the surfaces of S-Radel membranes soaked in 1.7 M vanadium ion solutions of different valance. The micrographs clearly show that only V^{5+} ions degraded the S-Radel membrane. Additionally, the S-Radel membrane exposed to V^{4+} (anolyte) and V^{2+}/V^{3+} (catholyte) did not undergo any degradation after 100 cycles (20 days run time) in a new Fe/V redox system, and postmortem analysis of the membrane showed no physical damage. The new Fe/V redox system employed 1.25 M V^{4+}/1.25 M Fe^{2+} (anolyte) and 1.25 M V^{3+}/1.25 M Fe^3 (catholyte) as electrolyte solutions (details of the study will be published elsewhere). V^{2+}, V^{3+}, and V^{4+} ions are believed not to have high enough oxidation power to degrade the S-Radel polymer because the standard potential of V^{3+}/V^{4+} and V^{2+}/V^{3+} redox couple is 0.337 and −0.255 V vs. NHE, respectively, significantly lower than 1.0 V vs. NHE for the V^{4+}/V^{5+} redox couple [24]. The potential of the V^{4+}/V^{5+} redox couple increases gradually with SOC, and steeply increases as SOC approaches 100%.

The S-Radel membrane soaked in the V^{5+} solution cracked into small pieces, likely due to a decrease in polymer molecular weight upon oxidation by V^{5+}. In comparison, for flow cell testing, the membrane underwent internal delamination preferentially on the side of the membrane that faced the positive electrode. Thus there appears to be different degradation modes whether the membrane is soaked in a quiescent solution or cycled in an operating VRFB.

3.3 Raman analysis of ex-situ degraded and in situ cycled S-Radel membranes

Representative Raman spectra from the S-Radel membrane that underwent 50 cycles in a VRFB are shown in Fig. 6.

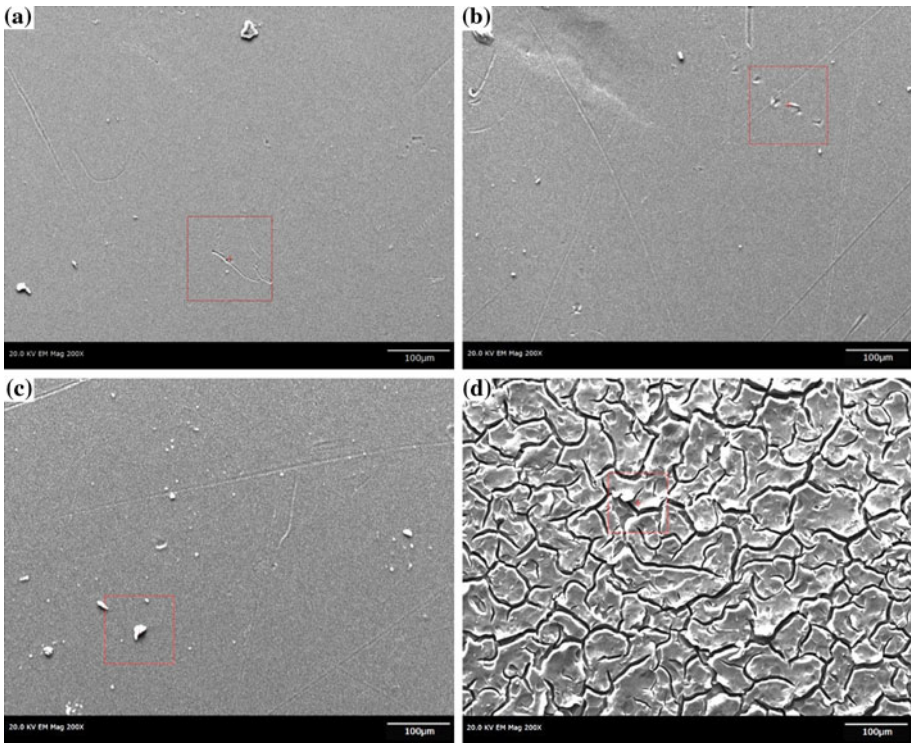

Fig. 5 Surface scanning electron micrographs of S-Radel membranes immersed at 40 °C in 1.7 M V^{n+} + 5.0 M SO_4^{2-}: **a** 100 h, V^{2+}; **b** 100 h, V^{3+}; **c** 40 days, V^{4+}; and **d** 80 h, V^{5+}

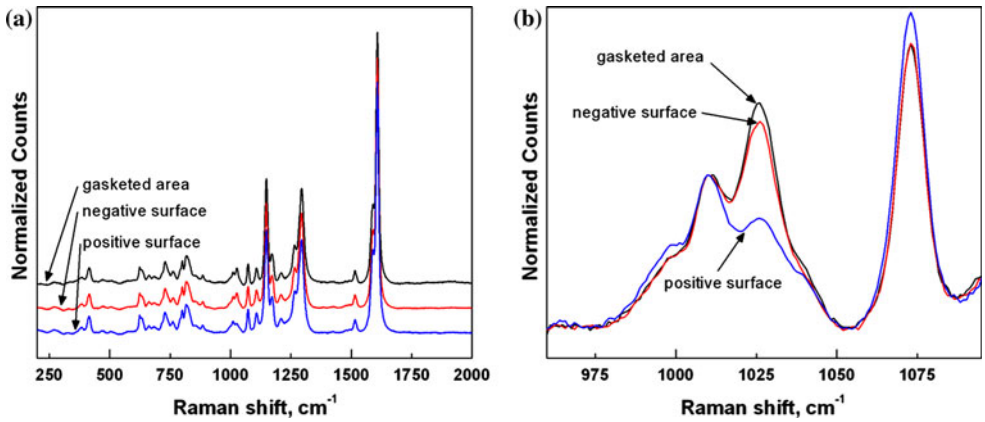

Fig. 6 Raman spectra of active area and gasketed area of the S-Radel membrane cycled 50 times

Overlaid spectra (Fig. 6a) of the gasketed area, membrane surface that faced the negative electrode, and membrane surface that faced the positive electrode, show that there is no significant detectable chemical degradation in the survey scans. Modes associated with aromatic C=C stretching (1600–1500 cm^{-1}), sulfone SO_2 stretching (1294, 1265, 1150 cm^{-1}), C–O–C stretching of the aryl ether (1205 cm^{-1}), aromatic ring vibrations (1110, 1073, 1010 cm^{-1}), and other features associated with aromatic C–H deformations and C–S stretches (below 1000 cm^{-1}) all remain unchanged within detection limits [25–31]. The only noted changes occurred at the sulfonate SO_2 symmetric stretch (1026 cm^{-1}). The high-resolution spectra shown in Fig. 6b were normalized to the ring vibration of *p*-substituted aryl ether at 1010 cm^{-1} and showed the effect that the 50 cycle test has on the sulfonate SO_2 stretch. In the high-resolution scans, differences were detected between the protected gasketed area and the active area of the membrane facing the positive and negative electrodes. The Raman data show that there is a detectable change in the SO_2 stretch for the surface of the membrane that faced the positive electrode. However, no other chemical changes were evident in other regions of the spectra.

Raman spectroscopy was also used to interrogate membranes immersed in different vanadium ion solutions. Figure 7 shows that there is a clear depression of the 1026 cm^{-1} band upon exposure to V^{5+} solution. This peak

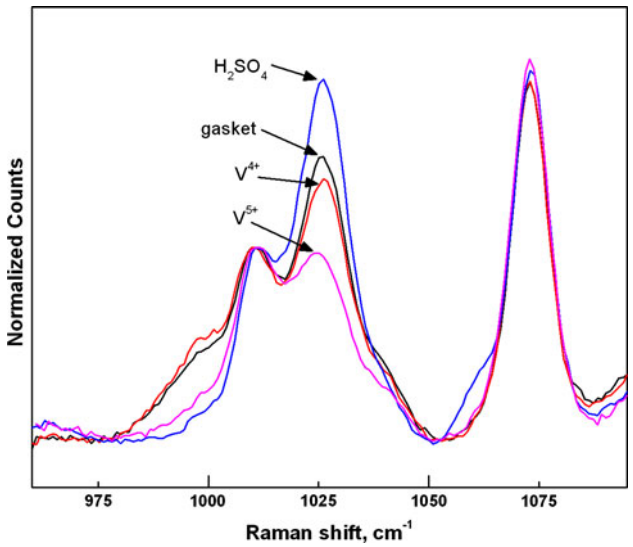

Fig. 7 High-resolution Raman spectra of gasketed area on S-Radel membrane cycled 50 times, and S-Radel soaked in H_2SO_4, V^{4+}, and V^{5+} ion solutions, respectively

is known to vary in both wavenumber and intensity depending on the counter ion present [25, 26, 28, 29]. The fully protonated membrane after immersion in H_2SO_4 showed the highest intensity peak. The gasketed area and the membrane exposed to V^{4+} solution showed less intense bands than the fully protonated sample, which was likely a result of vanadium ions displacing the acidic protons. The difference between the 1026 cm^{-1} band upon exposure to V^{4+} or V^{5+} could be due to some chemical degradation of the sulfonate groups or may be a consequence of different vanadium complexes at the sulfonate site. Taken together, the membrane breaking into pieces when exposed to V^{5+} solution and the depressed Raman band at 1026 cm^{-1} indicated that there was some chemical change in the samples exposed to V^{5+} ions while there was little or no chemical change in the membrane upon exposure to V^{4+} solution. The change in the 1026 cm^{-1} Raman band in the V^{4+} sample compared to a fully protonated sample was due to ion exchange. However, the change in the chemical structure of the membrane during degradation in V^{5+} solution or with cycling in a flow cell as observed by Raman (as well as by FTIR and NMR analysis, not shown) is slight.

3.4 Effect of flow cell state of charge on degradation

As polymer oxidation by V^{5+} ions is high near 100% SOC, the operation window (or SOC) is expected to have an effect on the extent of damage of the membrane. Flow cell cycling with two operation windows: 1) SOC 90/100% with 60 (78 h run time) and 250 cycles (240 h run time), and 2) SOC 0/10% with 80 cycles (78 h run time), was conducted. Figure 8a and b show surface scanning electron micrographs of the S-Radel membrane from the 250 cycle test, where liquid electrolyte on surfaces of the cycled S-Radel membrane was removed by gentle blotting with a laboratory wipe. The membrane surface adjacent to the negative electrode did not show any cracks or damage and EDS analysis confirmed that the particles on the surface were vanadium oxide precipitates from residual electrolyte. In comparison, the membrane surface adjacent to the positive electrode showed severe cracks, similar to what was observed for the membrane between 0 and 100% SOC for 50 cycles (Fig. 2d).

Figure 8c and d show the surface scanning electron micrographs of the S-Radel membrane cycled 60 times between 90 and 100% SOC and soaked in deionized water after disassembly. The surface in contact with the negative electrode remained intact, but the surface in contact with the positive electrode displayed severe cracking. In comparison, the S-Radel membrane cycled 80 times between 0 and 10% SOC and soaked in deionized water did not undergo any visible damage as shown in Fig. 8e and f. Maintaining a low SOC level decreases the electrolyte potential (1.03 V for 10% SOC vs. 1.22 V for 99% SOC) and therefore the low oxidation power of the solution may account for the negligible damage observed. These results demonstrate that membrane degradation can be reduced by operating VRFBs in a suitable SOC range.

3.5 Membrane resistance hysteresis

The discharge voltage of a flow cell with an S-Radel membrane was compared to that of a flow cell with a Nafion 117 membrane at various discharge current densities in Fig. 9a. The flow cell with the S-Radel membrane suffered from a voltage depression at high SOC levels and this anomalous voltage depression became more apparent as the discharge current increased. However, for the cell with a Nafion membrane, this type of voltage depression was not observed up to a current density of 100 mA cm^{-2}, where a very small depression was observed near 100% SOC. Figure 9b shows the ohmic resistance of the flow cell with the S-Radel membrane at different SOCs. The measured areal ohmic resistance was 1.1–1.25 Ω cm^2 over the whole range of SOC during the charging, however, the resistance increased by a factor of 1.5–2 at high SOC (70–95%) during discharging, which accounts for the observed voltage depression. In comparison, the flow cell with a Nafion membrane did not show hysteresis of the cell resistance during charge/discharge.

Cell ohmic resistance consists of an electronic contribution (graphite felt, solid current collector, and contact resistances) and an ionic contribution due to the membrane.

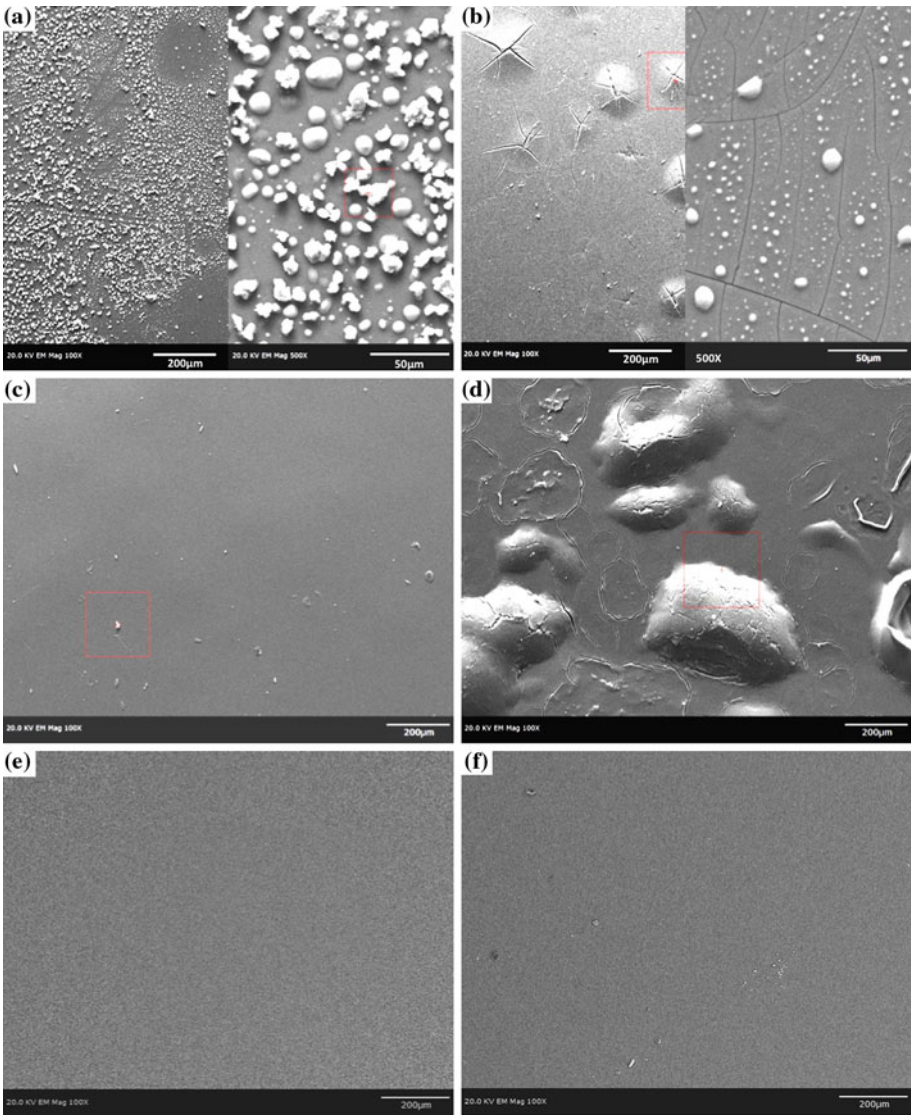

Fig. 8 Scanning electron micrographs of S-Radel membranes cycled between 90 and 100% SOC: **a** negative electrode side, not soaked in water, 250 cycles; **b** positive electrode side, not soaked in water, 250 cycles (220 h); **c** negative electrode side, soaked in water, 60 cycles; **d** positive electrode side, soaked in water, 60 cycles; **e** negative electrode side, soaked in water, 80 cycles; and **f** positive electrode side, soaked in water, 80 cycles

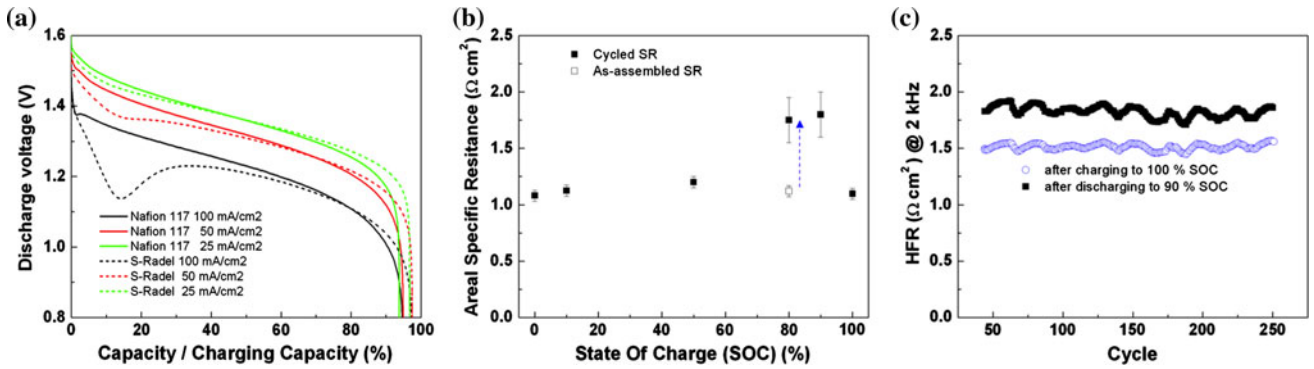

Fig. 9 Discharge curve and areal specific resistance of flow cell with S-Radel membrane: **a** comparison of Nafion 117 and S-Radel with different discharging current density; **b** areal specific ohmic resistance of S-Radel membrane with different SOC levels; and **c** high frequency resistance with cycles during cycling between 90 and 100% SOC

The ionic resistance dominates the cell resistance due to the high conductivity of the other components (the dry cell resistance without a membrane is 0.187 Ω cm^2, 16.7% of the cell resistance with the membrane). As shown in Fig. 9b, the ohmic resistance of an uncycled flow cell with a virgin S-Radel membrane and electrolyte solution (80%

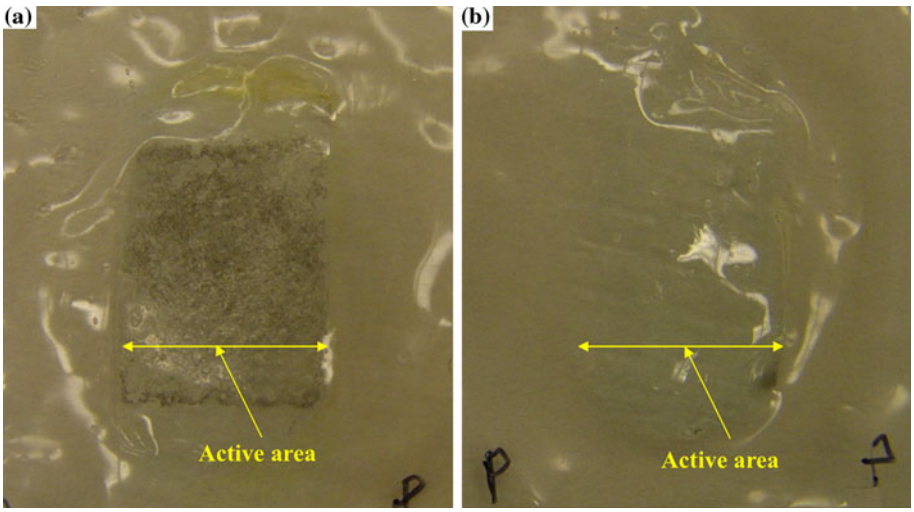

Fig. 10 Comparison of optical micrographs of the S-Radel membranes that underwent flow cell cycling for different SOC ranges: **a** SOC 90/100%, 60 cycles and **b** SOC 0/10%, 80 cycles

SOC) was $\sim 1.1\ \Omega\ cm^2$, much lower than that of the flow cell experiencing discharge ($1.8\ \Omega\ cm^2$). Figure 9c shows that the high resistance observed during discharge was recovered during the charge cycle.

Figure 10 shows optical micrographs of S-Radel membranes that underwent high and low SOC cycling where black particles were observed in the membrane for the 90/100% SOC tests. These particles were located inside the membrane as they could not be removed with surface rinsing by deionized water. It should be noted that the flow cell was disassembled in the discharged state, which had high membrane resistance and therefore, there could be some correspondence between the high resistance and particle formation. In comparison, the S-Radel membrane experiencing 80 cycles between 0 and 10% SOC did not contain any visible particles in the membrane. The in situ formation of non-conductive particles in the membrane during cycling could lead to the observed increase in membrane resistance. We hypothesize that these particles, which form and dissolve according to the observed increase and decrease of membrane resistance, likely weaken the membrane closer to the positive electrode, and in combination with chemical degradation by the V^{5+} ions, caused membrane delamination. It is also expected that these particles are likely related to the V-rich region observed in the 50 cycled membrane (Fig. 3b).

4 Conclusions

Degradation of a sulfonated poly(sulfone) membrane was investigated during VRFB cycling as well as in accelerated chemical stability immersion tests. In the flow cell cycling studies, the membrane suffered from delamination on the surface in contact with the positive electrode. In comparison, the membrane surface exposed to the negative electrode (V^{2+} and V^{3+} ion-containing solution) remained intact. A vanadium-rich and sulfur-deficient band was observed on the membrane surface that experienced delamination and Raman spectroscopic analysis of the surfaces of the membrane indicated a depressed 1026 cm^{-1} peak corresponding to the sulfonate SO_2 stretch for the degraded surface.

In the immersion tests, the S-Radel membrane immersed in V^{5+} ion-containing solution cracked into small pieces, likely due to a decrease in a polymer molecular weight upon oxidation by V^{5+} ions. On the other hand, the S-Radel membrane immersed in V^{2+}, V^{3+}, or V^{4+} ion-containing solution remained undamaged. The chemical damage was exacerbated in the concentrated V^{5+} ion-containing solution of 1.7 M, typically used in the VRFB, compared to a 0.1 M V^{5+} ion-containing solution. Raman analysis showed small chemical changes for the membrane exposed to V^{5+} ions, which was convoluted with changes in the 1026 cm^{-1} band due to ion exchange.

Even though the S-Radel membrane underwent severe mechanical damage during flow cell cycling, significant chemical degradation was not obvious by spectral analyses. The VRFB with the S-Radel membrane suffered abnormal voltage depression under discharge in the SOC range of 70–95%, which was not observed for cells with a Nafion membrane. This abnormal voltage depression was a consequence of the irregular increase of membrane resistance during discharge, which could be recovered by full charging. The membrane resistance hysteresis and severe mechanical degradation of the membrane during cycling may be due to local precipitation of solid particles inside the membrane. Coupled with changes in the polymer molecular weight upon exposure to V^{5+} ions, the mechanical stress imposed by cyclic formation of membrane precipitates could be a significant degradation mode for aromatic membranes under certain conditions in VRFBs.

Acknowledgments The work is supported by the Office of Electricity (OE Delivery & Energy Reliability (OE), U.S. Department of Energy (DOE) under contract DE-AC05-76RL01830. Solvay Advanced Polymers is acknowledged for the donation of Radel polymer. The authors thank Dr. Daiwon Choi and Dr. Tak Keun Oh for SEM/EDS analyses.

References

1. Yang Z, Liu J, Baskaran S, Imhoff CH, Holladay JD (2010) JOM 62:14
2. Eckroad S (2007) Technical report EPRI-1014836. Electric Power Research Institute, Palo Alto
3. Skyllas-Kazacos M (2009) Encyclopedia of electrochemical power sources, pp 444–453
4. Sun C, Chen J, Zhang H, Han X, Luo Q (2010) J Power Sources 195:890
5. Pivovar B, Yang Y, Cussler EL (1999) J Membr Sci 154:155
6. Kim S, Viswanathan V, Zhang J, Wang W, Li L, Yang Z (2010) In: 218th ECS meeting, Las Vegas, NV (abstract # 184)
7. Kim S, Yan J, Schwenzer B, Zhang J, Li L, Liu J, Yang Z, Hickner MA (2010) Electrochem Commun 12:1650
8. Sukkar T, Skyllas-Kazacos M (2004) J Appl Electrochem 34:137
9. Luo Q, Zhang H, Chen J, You D, Sun C, Zhang Y (2008) J Membr Sci 325:553
10. Luo Q, Zhang H, Chen J, Qian P, Zhai Y (2008) J Membr Sci 311:98
11. Zeng J, Jiang C, Wang Y, Chen J, Zhu S, Zhao B, Wang R (2008) Electrochem Commun 10:372
12. Schwenzer B, Kim S, Vijayakumar M, Yang Z, Liu J (2010) J Membr Sci 372:11
13. Hickner MA, Pivovar BS (2005) Fuel Cells 5:213
14. Chen D, Wang S, Xiao M, Meng Y (2010) J Power Sources 195:2089
15. Mai Z, Zhang H, Li X, Bi C, Dai H (2011) J Power Sources 196:482
16. Chen D, Wang S, Xiao M, Meng Y (2010) Energy Convers Manag 51:2816
17. Zhang S, Yin C, Xing D, Yang D, Jian X (2010) J Membr Sci 363:243
18. Kim J, Lee S, Choi S, Jin C, Kim J, Ryu C, Hwang G (2010) J Ind Eng Chem 16:756
19. Kim S, Yan J, Schwenzer B, Zhang J, Li L, Liu J, Yang Z, Hickner MA (2010) In: 218th ECS meeting, Las Vegas, NV
20. Mohammadi H, Skyllas-Kazacos M (1997) J Appl Electrochem 27:153
21. Dyck A, Fritsch D, Nunes SP (2002) J Appl Polym Sci 86:2820
22. Fujimoto CH, Hickner MA, Cornelius CJ, Loy DA (2005) Macromolecules 38:5010
23. Lawrence J, Yamaguchi T (2008) J Membr Sci 325:633
24. Bard AJ, Faulkner LR (2001) Electrochemical methods: fundamentals and applications. Wiley, New York
25. Johnson BC, Yilgor I, Tran C, Iqbal M, Wightman JP, Lloyd DR, McGrath JE (1984) J Polym Sci A 22:721
26. Sollinger S, Diamantoglou M (1997) J Raman Spectrosc 28:811
27. Pihlajamaki A, Vaisanen P, Nystrom M (1998) Colloids Surf A 138:323
28. Edwards HGM, Brown DR, Dale JA, Plant S (2000) Vib Spectrosc 24:213
29. Edwards HGM, Brown DR, Dale JA, Plant S (2001) J Mol Struct 595:111
30. Wang F, Hickner MA, Kim SY, Zawodzinski TA, McGrath JE (2002) J Membr Sci 197:231
31. Muthu Lakshmi RTS, Kumari R, Varma IK (2004) J Therm Anal Calorim 78:809